A reprogrammable and intelligent monitoring system for rock-collapse forecasting

Cesare Alippi, *Fellow, IEEE*, Giacomo Boracchi, Manuel Roveri

***Abstract*—The lack of clearly noticeable forerunners, the need to acquire large amounts of data coming from sensors sampled at mid/high rates and the potentially catastrophic effects of the physical phenomenon under monitoring make the rock collapse forecasting a challenging and valuable environmental monitoring application. In this paper we describe a rock-collapse forecasting system based on a hybrid wireless-wired architecture where a set of acquisition units are connected through a fieldbus to a base station, which collects and wirelessly transmits acquired measurements to a remote control room. The main features of the proposed rock-collapse forecasting system are the ability to process locally and in real-time data sampled at high-frequency rates; the run-time remote reconfigurability of the forecasting application; the possibility to distribute the intelligent processing through the system layers to balance energy consumption and application performance. Five instances of the proposed system have been deployed along the Swiss-Italian Alps.**

***Index Terms*—Distributed monitoring systems, hybrid sensor networks, remote reconfigurability, high-frequency sampling rock collapse forecasting, intelligent monitoring systems.**

I. Introduction

Among the wide range of physical phenomena threatening mountain regions, the collapse of rock faces represents one of the most dangerous and hard to predict. In fact, rock collapse is characterized by a rapid dynamic just before the fall and might induce catastrophic effects whenever human settlements, roads or critical infrastructures are affected. For these reasons, an effective and real-time monitoring and forecasting action is required to promptly raise alarms and possibly activate emergency procedures.

Environmental forces such as those induced by thermal stress, frost/defrost cycles during the winter and gravitation significantly contribute to the fall but their role is only partly understood. From a geophysical perspective, rock collapse is the final phase of a continuous process induced by the coalescence of *micro fractures* into larger ones. Interestingly, during this coalescence phase, microacoustic emissions i.e., burst signals resembling in shape those generated by earthquakes, are emitted whenever a fracture enlarges its size. These bursts represent extra information that a suitable monitoring system can acquire to open further views on the physical phenomenon under observation. Microacoustic emissions are characterized by mid/high sampling rates; we bounded the sampling frequency to 2kHz, frequency coarsely associated with evolving millimetric-size fractures. The choice implies that we observe burst signals with spectrum up to 1kHz, a reasonable frequency according to geophysicists. This design constraint is appropriate since it is known that frequencies progressively reduce when getting closer to the rock fall [1].

The authors are with the Dipartimento di Elettronica e Informazione, Politecnico di Milano, Milano, Italy e-mail: firstname.lastname@polimi.it

The proposed rock collapse forecasting system is based on the hybrid wireless-wired hardware solution for structural health and environmental monitoring applications presented in [2]. The peculiar characteristic of the hardware is the combined use of wireless and wired communication: sensing units are connected through a fieldbus to a base station, which wirelessly transmits acquired data (or features/events extracted from them) to a control room. By relying on such a hardware architecture we developed a novel rock collapse forecasting system whose distinctive features are:

- the ability to *acquire and locally process* multiple scalar signals with a sampling rate up to 2kHz;
- the presence of an *intelligent processing* distributed through the network aiming at reducing the overall energy consumption, while maintaining the application performance. A first level consists in a local trigger that analyses online the acquired data to identify those events that are worth to be remotely transmitted. Another intelligent mechanism autonomously switches the working modality of the monitoring system between normal (periodic transmission) and alarm mode (a potentially critical situation). Finally, intelligence is considered at the event-classification level in the control room where false alarms are automatically discarded;
- the *reprogrammability* of the application at runtime, that is, the ability to modify or update the software code and/or the parameters of the sensing units;
- a two-layer synchronization mechanism for hybrid wireless-wired sensor networks guaranteeing a strict synchronization among the acquisition units (less than 1ms).

We emphasize that we currently have five operational deployments of the proposed system for rock-collapse forecasting in Northern Italy and Switzerland; details of these deployments are given in Table I. Since the analysis of microacoustic emissions for rock collapse forecasting is still a novel and challenging research area, the design and development of these systems required a strict collaboration with the experts of the field (i.e., geologists and geophysicists). Remarkably, data acquired by our systems represent valuable information both from the geological/geophysical point of view (to improve the geological/geophysical knowledge about the collapse of rock faces) and from the technological point of view (to increase the effectiveness and the robustness of our systems).

This paper significantly extends a preliminary version of the system presented in [3] and is organized as follows.

Deployment	*Geographical area*	*Active since*	*Number of Units*
St. Martin mount	Lake Como area (Northern Italy)	Apr. 2010	8
Rialba's tower	Lake Como area (Northern Italy)	Jul. 2010	3
Val Canaria	Canton Ticino (Switzerland)	Oct. 2011	2
Gallivaggio	Valchiavenna (Northern Italy)	Sep. 2012	5
Premana	Valvarrone (Northern Italy)	Oct. 2012	3

TABLE I
DEPLOYMENTS OF THE PROPOSED SYSTEM FOR ROCK-COLLAPSE FORECASTING IN NORTHERN ITALY AND SWITZERLAND.

Section II describes the related literature, while Section III introduces the system architecture for the proposed monitoring system. The hardware, operating system, communication, service and intelligent application layers are detailed in Section IV, V, VI, VII and VIII, respectively. Section IX describes the experimental results of the proposed system in terms of application performance and quantifies the gain introduced by the intelligent processing layer.

II. RELATED LITERATURE

Although the collapse of rock faces represents a harmful natural hazard, the lack of clear forerunners and the difficulty of the deployment limit the number of existing available monitoring systems. To the best of our knowledge there is only one another recent system acquiring acoustic emissions for the monitoring of mountain walls [4]. Therefore, in order to provide a more comprehensive state of the art, we also present monitoring/forecasting systems based on wireless solutions addressing similar scenarios (e.g., structural monitoring, seismic or volcanic eruption monitoring). The comparison focuses on some key aspects, namely, the nature of the local and the distributed processing, the sampling rate, the availabilty of synchronization mechanisms and the reprogrammability ability.

An acoustic-emission monitoring system designed to operate on Alpine rock walls is presented in [4], where a threshold-based triggering mechanism is used to extract acoustic events. Features are extracted from events and remotely transmitted to a control room only upon request. The sampling rate is 500kHz. Details about the considered synchronization algorithm are not provided and reprogramming mechanisms are not considered in this system.

An heterogeneous system for structural health monitoring based on Wireless Sensor Network (WSN) units and wired cameras is suggested in [5]. The software architecture relies on TinyOS [6]; the sampling frequency is 100Hz. A threshold-based detector is considered at the unit level and the synchronization relies on the Timing-sync Protocol for Sensor Networks [7]. No reprogramming mechanisms are considered.

WISDEN [8] relies on a WSN solution for structural health monitoring: it is based on TinyOS and the sampling frequency is 160Hz. The system relies on a threshold-based event detection mechanism and exploits a wavelet-based compression technique to reduce the communication bandwidth. WISDEN implements an ad-hoc data time-stamping scheme for the synchronization of acquired data. No reprogramming mechanisms for the units are available.

A WSN-based structural health monitoring system named SENTRI is presented in [9]. The considered operating system is TinyOS and the sampling frequency is 200Hz. Due to the peculiar in-line architecture (the system is organized as a line of 64 sensors), SENTRI relies on a 64-hop routing protocol. The synchronization mechanism is based on the Flooding algorithm [10]. Units cannot be remotely reprogrammed.

WISAN [11] is another intelligent WSN for structural health monitoring. Differently from previous solutions, WISAN relies on computational intelligent mechanisms and wavelet compression to make network units autonomous and reduce the bandwidth consumption, respectively. The system relies on an ad-hoc scheduler, while the sampling rate is 50Hz.

A time synchronized and reconfigurable WSN for structural health monitoring is described in [12]. There, the network units run FreeRTOS as operating system; the sampling frequency is 200Hz, and the event detection relies on a modal analysis. Acquisition parameters can be updated during the operational life through remote commands. An ad-hoc synchronization algorithm, called $\mu - Sync$, guarantees a very strict synchronization among the network units (below $10\mu s$).

TERRASCOPE is a down-hole seismic monitoring system proposed in [13]. It is composed of independent sensing units sampling at 250Hz and connected to a gateway through a field bus. The units rely on a customized scheduler and the gateway runs a Linux OS. TERRASCOPE allows to update the code running on the units by means of an additional digital bus. Events are detected through a trigger-based algorithm and clock synchronization relies on a GPS timer.

A WSN-based monitoring system for volcanic eruptions is described in [14]. The system is based on TinyOS and the sampling frequency is 100Hz. The synchronization mechanism is based on the Flooding algorithm. The system allows to update its operational parameters through the execution of remote commands, while the detection of events is based on the comparison between two exponentially weighted moving averages of incoming signals.

From the literature it comes out that existing solutions for structural health and environmental monitoring are generally not able to satisfy the sampling frequency as required by a rock collapse forecasting application. In addition, remote re-programmability and intelligent solutions for balancing energy consumption and application performance are seldom considered, hence still representing an open and cutting-edge research challenge. In contrast, the rock collapse forecasting system here proposed is able to acquire and process signals with sampling rates up to 2kHz and encompass both basic reprogramming mechanisms and intelligent processing as detailed in Section VII-A and in Section VIII, respectively.

III. THE SYSTEM ARCHITECTURE

The proposed rock collapse forecasting system is composed of a *Remote Monitoring System* (RMS) deployed on the rock face and a *Control Room* that collects data from the RMS for

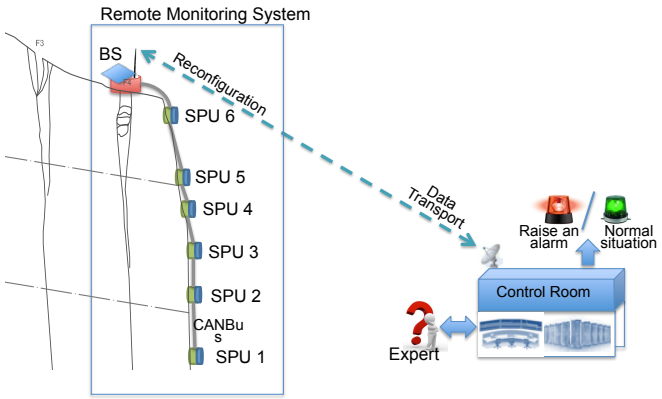

Fig. 1. The proposed rock collapse forecasting system.

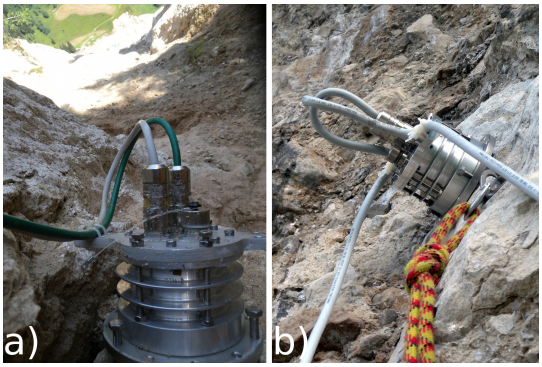

Fig. 2. SPUs in two deployments: a) Val Canaria b) Rialba's tower

subsequent storage, processing and interpretation. As shown in Fig. 1, the RMS is composed of a set of Sensing and Processing Units (SPUs) that are connected through a CAN bus to a Base Station (BS). SPUs are endowed with sensors to acquire micro-acoustic emissions (e.g., MEMS accelerometers, geophones) as well as more traditional sensors (e.g., inclinometers, temperature sensors, strain gauges). The BS collects data from the SPUs and transmits them to the Control Room.

From the hardware point of view, the proposed rock-collapse forecasting system is characterized by a large heterogeneity in terms of devices, technologies and performance. SPUs are low-power high-performance digital signal-processing units able to acquire, locally process and extract information of interest from the datastream sampled at 2kHz. Examples of SPUs are shown in Fig. 2. The BS provides both the power supply and the synchronization of the SPUs by means of the CAN bus, while the Control Room is composed of Personal Computers and servers organized into a typical internet-based service-oriented network architecture. From the software point of view, the system reflects the hardware heterogeneity where several different software modules and mechanisms cooperate to achieve the targets of the forecasting application.

With reference to Fig. 3, the architecture of the system comprises:

- the *hardware layer*, that provides the physical mechanisms for data acquisition, processing and transmission;

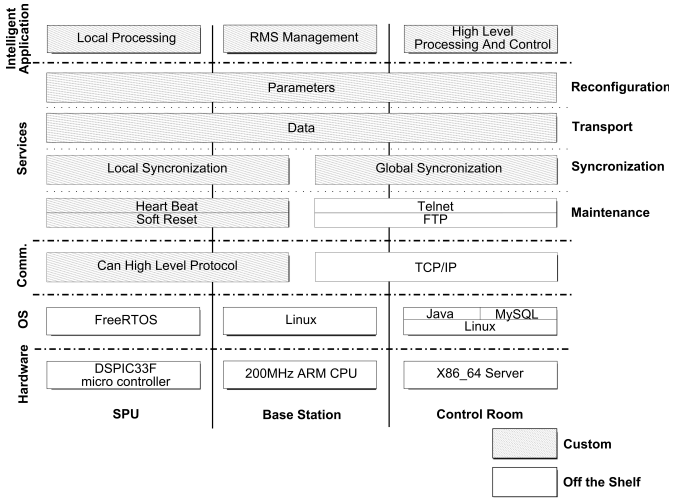

Fig. 3. The system architecture of the proposed rock collapse forecasting system.

- the *operating-system layer*, providing basic software functionalities to higher levels. It mainly consists in the operating-system services;
- the *communication layer*, providing the basic mechanisms supporting the local communication between SPUs and the BS via CAN bus and the remote communication between BS and Control Room by means of a WiFi/UMTS protocol;
- the *service layer* providing those services supporting the system reconfiguration, the data transport and the clock synchronization functionalities;
- the *intelligent application layer*, that makes available those functionalities allowing the monitoring application to be adaptive and autonomous.

Due to the peculiar application constraints and the large heterogeneity of the devices, the design of the software required an engineering approach where each software module (together with the interaction with other modules) has been carefully developed and tested from the functional and energetic point of view. To achieve this goal, the designed system relies on a layered architecture where each layer exploits the functionalities provided by lower ones to expose functions and mechanisms to upper layers. Unlike a vertical "cross-layer" system design, where functionalities are tailored to the specific hardware and layers are cross-designed to optimize performance (e.g., aggregation and fusion), a layered architecture is easier to design, test and maintain. In fact, each layer can be tested separately (black box testing) and an internal modification (not involving the interfaces) does not affect the other layers. Moreover, a layered architecture allows us to easily reuse the code in applications running on different hardware, whereas "vertical" approaches are generally application-specific and hardware-dependent.

As a final remark, we emphasize that each layer is designed to offer its functionalities to upper levels, minimizing both computational complexities and memory requirements. The layers of the proposed architecture are detailed hereinafter.

IV. The Hardware Layer

As described in the previous section, the proposed rock collapse forecasting system is based on a set of SPUs that are connected through the CAN bus to the BS, whose goal is to remotely transmit acquired information to the Control Room through a wireless connection.

SPUs gather sensor measurements, perform a local processing to extract features from acquired data and apply local classification to select only those microacoustic signals worth the transmission to the BS. For this reason, SPUs must remain always active (i.e., 100 % duty cycle), while the BS can be switched off to reduce the energy consumption (the adjustable duty-cycling mechanism of the BS is described in Section VIII-B).

SPUs are composed of two boards and a set of sensors. The first board, based on the 40Mhz Microchip DSPic33F microprocessor (256kB ROM and 30 kB RAM memory), performs the processing and communication tasks. The second board contains the signal conditioning circuits for the envisaged sensors. The sensor set comprises MEMS accelerometers and geophones for microacoustic burst inspection as well as more traditional sensors such as a temperature sensor, an inclinometer, and a strain gauge. SPUs do not have local energy harvesting capabilities and are powered by the BS through the CAN bus power lines.

The BS plays a fundamental role in the RMS since it coordinates the communication activity among SPUs and acts as a gateway between the RMS and the Control Room. The hardware platform of the BS comprises: the main board (based on a 200MHz ARM9-based PC104 board with 32MB RAM memory) executing the application at the BS level; the energy harvesting and management boards for energy acquisition through photovoltaic cells and energy management; the shutdown/wakeup board and the radio module (radio link/3G UMTS modem). The BS is endowed with rechargeable batteries (Lead Acid 12V 40Ah) and solar panels (polycristalline 20W nominal).

Finally, the Control Room has a radio module to communicate with the BS and hosts a database and an application server exposing typical service-oriented network facilities.

Further details about the hardware specifications and the energy consumptions can be found in [2].

V. Operating-System Layer

The Operating System (OS) layer optimizes the use of hardware resources and provides functionalities to the upper levels of the system architecture.

Among the wide range of OSs for embedded systems (e.g., [6], [15], [16]) we selected FreeRTOS [17] for the SPUs since it is multitasking, real-time, modular and officially supported by the considered micro-controller. These features perfectly fit the needs of our application.

As described in Section IV, the main board of the BS relies on a PC104-based embedded computer; for this reason, we decided to adopt Linux as the OS. Specifically, we configured a custom Debian distribution for ARM (based on kernel 2.6) to get a fast boot and shutdown (i.e, 1.9s) and a small flash memory occupation ($\sim$100Mbytes).

The OS layer of the Control Room relies on a standard Debian GNU/Linux 5.0 distribution for X86_64 microprocessors.

VI. Communication Layer

The aim of the communication layer is to provide data structures and services that allow the transmission of data and parameters among the SPUs, the BS and the Control Room. The communication layer is organized in two modules addressing the *local communication* between the BS and the SPUs and the *remote communication* between the BS and the Control Room.

A. Local communication

Local communication relies on the CAN field bus that represents a standard for wired transmissions in several critical applications such as industrial process control or automotive [2], [18]. We selected CAN bus among different technological solutions e.g., RS485, Industrial Ethernet, ProfiBus, ControlNet, for two main reasons. First, it is an open standard. Second, CAN hardware controllers are embedded in many off-the-shelf micro-controllers and industrial PCs (as such, it does not require additional hardware and software modules e.g., like Profibus).

The CAN hardware controllers available on the market generally provide the Physical and the MAC layer, while there are several options for the CAN bus-based routing protocol such as CANopen [19], DeviceNet [20], CAN Kingdom [21]. Unfortunately, these routing protocols suffer from two main problems. First, they generally rely on an master-slave mechanism with a special node or *master*, providing all services needed to control the network. Other nodes, or *slaves*, only send data to the master node. Unfortunately, this approach requires the master to be always active and duty-cycling energy saving approaches cannot be considered for the master node (as mentioned in Section III the BS requires a duty-cycling mechanism to reduce the energy consumption). Second, CAN bus routing protocols are generally designed to deliver a single-packet message accounting for 8Bytes payload for a CAN message. This is a critical point since the amount of data to be transmitted on the CAN bus is up to 8KByte (containing acquired measurements and system status information).

To solve the above problems we designed an ad-hoc routing protocol able to effectively manage the wired communication between the SPUs and the BS and, at the same time, keep under control the energy consumption. The proposed protocol is based on a polling approach, with the BS acting as the master node: each wired transmission is started by the BS which can either retrieve data from a SPU (*PULL-data protocol*) or dispatch a parameter update to a SPU (*PUSH-data protocol*). The BS periodically queries all the SPUs of the network one after the other. The polling phase ends when the BS has completed the PUSH/PULL protocols for all SPUs.

We divided data into CAN messages by creating the concept of *transaction* and building a framework similar to a TCP protocol.

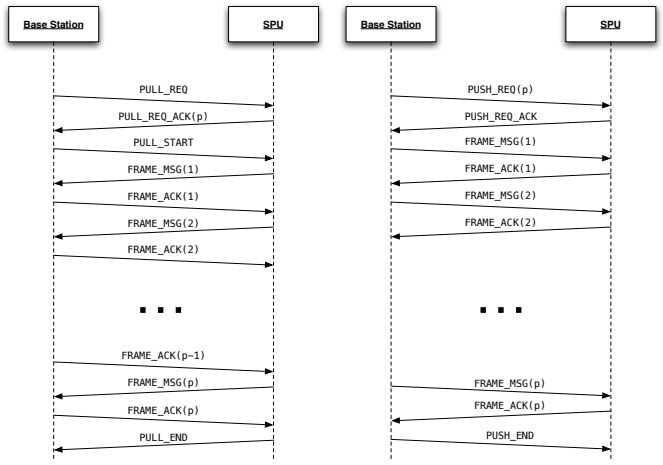

(a) Pull-data routing protocol (b) Push-parameters routing protocol

Fig. 4. The UML sequence diagrams of the proposed pull-data and push-parameters routing protocol for the CAN bus, respectively

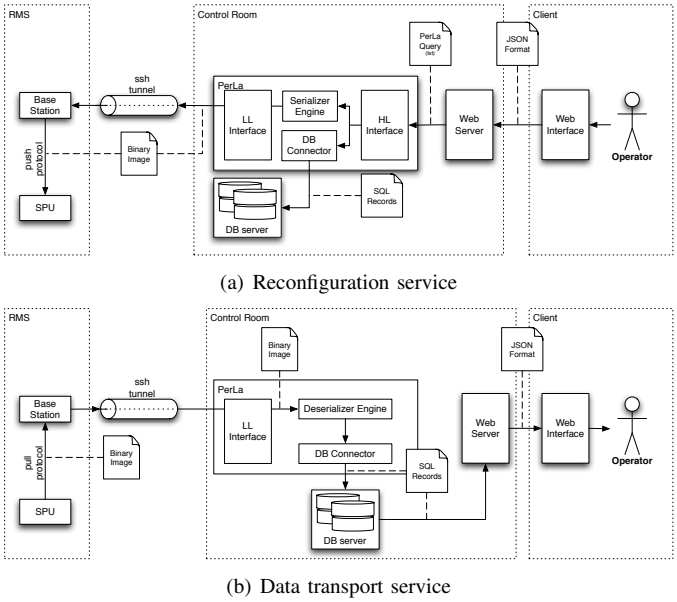

(a) Reconfiguration service

(b) Data transport service

Fig. 5. Reconfiguration and data transport service of the Service Layer

In the *PULL-data protocol*, whose UML sequence diagram is shown in Fig. 4(a), the BS initiates the transaction by sending the `PULL_REQ` message to an SPU, which replies with the `PULL_REQ_ACK` message specifying the number of data packets `p` to be transmitted. Then, the BS sends the `PULL_START` message to notify the SPU that it is ready to receive the data frames. For each `FRAME_MSG` sent by the SPU, the BS acknowledges the receipt with the `FRAME_ACK`. We emphasize that both messages specify the sequence number of the data frame which is currently transmitted or acknowledged. After the acknowledgment of the last data frame, i.e., the SPU receives the `FRAME_ACK` associated with the last `FRAME_MSG`, the SPU sends the `PULL_END` message to the BS to terminate the transmission. Afterwards, the SPU exits the protocol. Similarly, after the receipt of the `PULL_END` message, the BS exits the protocol. The *PUSH-parameter protocol* is the dual of the *PULL-data protocol* and its UML sequence diagram is shown in Fig. 4(b).

B. Remote communication

The remote communication is based on a long-range wireless transmission making use of either a WiFi dedicated radio link or a GPRS/UMTS mobile-based link. This remote communication module relies on a standard TCP/IP protocol endowed with a *tunneling* procedure aiming at encrypting data and parameters (during the transmission) and creating a virtual private network between the BS and the Control Room.

VII. Service Layer

The service layer provides the reconfiguration, data transport and synchronization functionalities to the sensor network.

A. Reconfiguration

Several parameters are associated to each SPU allowing the units to undergo reconfiguration both at the data acquisition and the signal-processing phases. Likewise, the BS can be reconfigured through a set of parameters, mainly associated with the duty-cycling activity. The *Reconfiguration* service permits the operator to modify the SPUs and BS parameters and, hence, the interaction of the system with the environment as well as its internal functional behavior.

This feature is particularly relevant in systems operating in harsh environments and, even more, when little a priori knowledge about the phenomenon under investigation is available. For instance, we can modify the parameters associated with the intelligent application layer (shown in Table III), activate/disable acquisition channels for energy consumption reduction, modify the sampling rate depending on the carried information content. An overview of the reconfiguration service workflow is presented in Fig. 5(a).

The reconfiguration service is composed of three modules:

- the operator front-end: a web application that, in execution at the control room and accessible to authorized users, permits to change the system parameter configuration through a web browser. By means of a Web Interface that shows the set of tunable parameters the operator can select the target unit to be updated and the new set of parameters;
- the middleware: a JAVA application running at the Control Room that transforms the operator decisions into commands to be sent to the remote system. Among the available middleware for sensor networks [22]–[25], we adopted PerLa [26]. PerLa, designed in our institute, is a general-purpose middleware for distributed systems aiming at presenting a standard and abstract interface to data and parameters of network devices. Differently from other middleware solutions, PerLa provides a database-like abstraction for the network elements and guarantees a full support for heterogeneity at the hardware/sensor level, both at runtime and at deployment time;
- the back-end: the software, running at the BS, enables both the update of the parameters affecting the BS and dispatches those to be delivered to the target SPU. More

specifically, parameters are updated only if different from the previous values. To transmit the new set of parameters we rely on the PUSH-data protocol described in Section VI.

B. Data Transport

Data transport is the service responsible for delivering acquired data from SPUs to the Control Room. The service workflow, described in Fig. 5(b), provides mechanisms to address the SPU-to-BS and BS-to-Control Room transport phases.

In the SPU-to-BS phase, the data transport is based on the PULL-data protocol described in Section VI-A. The data frame represents the image of the in-memory structure used by SPU to store the acquired measurements.

In the BS-to-Control Room phase, the BS connects to the Control Room via the TCP-IP channel described in Section VI-B and transmits the data-frames collected from the SPUs.

C. Clock Synchronization

The clock synchronization among the SPUs of the RMS is crucial to guarantee an effective analysis of the gathered data in high-frequency applications. In fact, the localization of a micro fracture within a rock face relies on the analysis of highly synchronized micro-acoustic bursts (i.e., with a maximum clock skew of 1ms).

The complexity of the hardware architecture of the proposed forecasting system forced us to address the problem of synchronization into two separate phases:

- *global synchronization*: the SPUs, the BS and the Control Room are synchronized by means of the *Network Time Protocol* (NTP) [27] whenever the BS remotely connects to the Control Room;
- *local synchronization*: the SPUs are synchronized by means of an ad-hoc synchronization protocol in between two connections of the BS with the Control Room. Remarkably, the synchronization among the SPUs can take part even when the BS is switched off for duty-cycling.

The global synchronization mechanism guarantees that all SPUs are synchronized with the clock of the Control Room whenever the remote communication is established. To accomplish this task the BS and the Control Room rely on an NTP client for clock synchronization (i.e., the NTP client connects to the NTP server to get the *Internet clock*). Afterwards, the BS propagates the updated time to all the SPUs through a high-priority broadcast message that, once received, permits the SPUs to update their internal clocks.

Differently, the local synchronization guarantees the synchronism among SPUs. In fact, when the BS is switched off during duty-cycling SPUs keep on synchronizing themselves to minimize the clock skew by means of the local synchronization mechanism: one of the SPU, i.e., the *synchronization master*, that can be either fixed in hardware or remotely defined by the Control Room, periodically broadcasts a synchronization message to all SPUs.

Both in local and global synchronization we introduced a mechanism to compensate the delay caused by the propagation time of the synchronization messages on the CAN bus. Remarkably, this delay T_d is a deterministic offset which depends on the propagation time of the broadcast message on the CAN bus. This delay has been considered common to all SPUs since we experimentally evaluated that the difference of the propagation delays among the SPUs was negligible.

Delay T_d can be easily computed since it depends on the number of bits N_{CAN2b} of the synchronization message, the transmission baud-rate f_{br} and the message processing time T_{IRQ} of the SPU micro-controller, i.e.,

$$T_d = \frac{N_{CAN2b}}{f_{br}} + T_{IRQ}. \quad (1)$$

T_{IRQ} is generally negligible compared to $\frac{N_{CAN2b}}{f_{br}}$, because the interrupt routine associated with the synchronization messages is executed in about 500 clock cycles (with a 40MHz clock). The size N_{CAN2b} of the synchronization messages is 130 bits including the CAN bus identifier, the payload, the CRC and other fields. As an example, by relying on Eq. 1, the propagation delay T_d with $f_{br} = 125$Kbps and $f_{br} = 250$Kbps are 1.04ms and 0.52ms, respectively. To compensate this delay, in the interrupt routine, the value of T_d corresponding to the specific baud-rate is added to the timestamp received from the Master Sync (both local or global).

It is noted that, for burst-localization purposes, global synchronization is less important than the local one. In fact, local synchronization is fundamental to keep the SPUs synchronized to correlate the acquired micro-acoustic emissions (e.g., by estimating the arrival time of the acquired burst). Clearly, a common drift for all SPUs does not affect this analysis, which, on the contrary, can be totally compromised by a clock skew among SPUs. For this reason we opted for a simple NTP mechanism for global synchronization.

The timing format is the Coordinated Universal Time (UTC) [28] measured with a granularity of the microsecond. A more effective two-way synchronization procedure e.g., see [29], could be considered in more critical situations requiring a very strict synchronization.

VIII. Intelligent Application Layer

The application layer provides intelligent tools for acquiring, transmitting and processing micro-acoustic emissions at the SPUs, the BS and the Control Room levels. Table II summarizes the intelligent mechanisms adopted by the application layer.

The SPUs implement a trigger mechanism based on sliding windows to store only micro-acoustic emissions characterized by a suitable magnitude, since fractures typically yield an energy content that is far larger than most of background signals. All the SPUs convey bursts, i.e., micro acoustic emissions stored at the SPUs and delivered through the whole system, to the BS, which is in charge of delivering them to the Control Room over the wireless channel. When the BS is in *normal transmission-mode*, these communications are scheduled in a periodic way, to reduce the number of wireless radio activations because of energy constrains. However, the

Unit	Prior Information	Solution
SPUs	Micro-acoustic emissions related to fractures have large magnitude	Bursts are stored depending on a trigger on signal energy applied to running windows
BS	Micro-acoustic emissions related to fractures yield several bursts	Counting bursts arrivals in a short time interval to anticipate the transmissions to the Control Room
Control Room	Burst related to fractures have distinctive shapes	LDA in feature space to discriminate false alarms and possible fractures

TABLE II
THE MECHANISMS CONSIDERED IN THE INTELLIGENT APPLICATION LAYER AT THE DIFFERENT SYSTEM UNITS

BS might switch to an *alarm transmission-mode* when a large number of bursts arrives from the SPUs within a short interval of time, as this might indicate a significant activity within the rock face and possibly a critical situation. In these cases bursts are delivered to the Control Room before the scheduled time. The core of the monitoring activity is executed at the Control Room, where bursts are processed by extracting features to automatically identify false alarms and submit to the visual inspection of the geophysicist only bursts that possibly indicate fractures. A suitable feature subspace for burst separation is learned by means of Linear Discriminant Analysis (LDA) [30], computed over a training set of supervised bursts.

These intelligent mechanisms are described and commented in the rest of the section, while Table III summarizes their main parameters.

Param.	*Description*	*Device*	*Default value*
l	Length of the long window for event detection	SPU	32 samples
s	Length of the short window for event detection	SPU	128 samples
Γ_T	Threshold for event detection	SPU	3
L	Number of samples stored in each bursts	SPU	128 samples
W_B	Length of the time window to count recent burst arrivals	BS	180s
d	Transmission period in normal transmission mode	BS	7200s
Γ_F	Threshold on the samples acquired in W_B to switch to the alarm-transmission mode	BS	3
Γ_B	LDA threshold to distinguish between bursts and false alarms	Control Room	3.8

TABLE III
MAIN PARAMETERS OF THE INTELLIGENT APPLICATION LAYER

A. Intelligent application layer: the SPU

The application in execution at the SPUs has been organized to address three main tasks: data *acquisition*, *processing* and *communication*. During acquisition, data are acquired by three-axial accelerometers (MEMS) and geophones, which are sampled at 2kHz. Data are converted by the internal 12bit ADC and stored into a memory buffer.

The processing phase is activated after the storage of each burst, and consists of a digital filtering followed by a triggering mechanism. First, each of the three channels of the MEMS/-Geophone recordings are processed through parametric high-pass Finite Impulse Response (FIR) filters. Then, events are detected by comparing the mean squared amplitude of the signal over two different-sized sliding windows, as in [31]. In particular, if we denote by $\bar{x}_l$ the average squared amplitude over a large window of l samples (e.g., $l = 128$), and $\bar{x}_s$ the average squared amplitude over a short widow of s samples (e.g., $s = 32$), an event is detected when $\bar{x}_s/\bar{x}_l$ exceeds a user-defined threshold Γ_T, that has been experimentally set to 3. Larger values would possibly discard true micro acoustic emissions, while smaller values would result in the unnecessary storage of false alarms (mainly induced by noise), hence causing to quickly fill the SPU memory.

The number of samples stored in each bursts is L, which is defined by the sampling rate and the bursts acquisition time. At 2kHz, values of L equal to 128, 256, 512 and 1024 correspond to acquisition times of 64ms, 128ms, 256ms and 512ms, respectively. If needed, acquisition time can be eventually extended up to 4s through down-sampling. The maximum number of events that can be stored is determined by the RAM capacity of the SPU (7460 bytes): when the memory is about to saturate only condensed information of each burst (such as timestamp, signal peak value, $\bar{x}_s$ and $\bar{x}_l$) is stored.

Besides MEMS and geophones, which acquire high-frequency bursts, SPUs are equipped with temperature, strain gauge and three-axial clinometer sensors. These sensors provide low–bandwidth signals, which are acquired at regular time instants and processed by means of a parametric FIR low-pass filter.

The application layer has been designed to guarantee the possibility to change the application at the SPUs at run-time through remote commands sent from the Control Room and the PUSH-data protocol described in Section VII-A. For instance, digital filters could be remotely enabled/disabled and application parameters (such as l, s, Γ_T and L) could be updated.

B. Intelligent application layer: the BS

The application layer at the BS aims at coordinating all the activities of the RMS: the BS collects data (including bursts) from the SPUs by means of the PULL-data protocol described in Section VII-B. Then, the BS remotely transmits data to the Control Room by means of the Remote Communication protocol described in Section VI-B. In normal transmission-mode, the BS communicates periodically with the Control Room to reduce the number of radio-module activations (thus lowering the energy consumption). Periodic transmissions (e.g., every d=7200s) guarantee a good trade-off between RMS throughput and energy consumption but might introduce a delay in critical or dangerous situations (e.g., when several micro-acoustic emissions are acquired in a very short time). Hence, the BS autonomously counts the number of bursts C_F over a window W_B of the most recent time instants (e.g., $W_B = 180s$). As soon as this value exceeds a threshold Γ_F, the BS switches into the alarm transmission-mode and immediately delivers

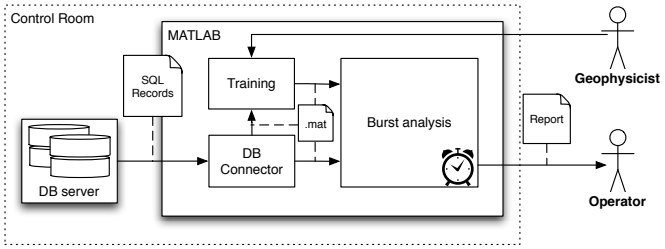

Fig. 6. Burst classification post processing work flow at the control room

bursts gathered from the SPUs to the Control Room. The BS remains in the alarm transmission mode up to when $C_F \geq \Gamma_F$. When C_F decreases below Γ_F, the BS returns to the normal transmission-mode. Γ_F has been experimentally fixed to 3. Smaller values of this threshold would result in an unnecessary activation of the alarm modality, while larger values would induce a delay in its activation in emergency situations.

In addition, the application at the BS dispatches commands (received from the Control Room) to specific SPUs and applies power-management policies depending on the energy availability (which is measured by its embedded hardware [2]). The period d characterizing the normal transmission-mode and the threshold Γ_F can be modified from the Control Room. The application at the BS also checks the exit status of all the utilities to diagnose remote connection failures and other errors. Errors and warnings are recorded in a log file, which is sent to the Control Room for diagnosis purposes.

C. Intelligent application layer: the Control Room

The application at the Control Room provides data storage (through an open-source relational SQL database MySQL Server 5.1), presentation (through the Spring framework running on top of a Tomcat application server) and intelligent processing of acquired measurements implemented in MathWorks MATLAB.

The application is composed of a *web application*, to remotely visualize the recorded bursts and a local MATLAB application, which implements an intelligent mechanism to separate bursts that can be safely considered *false alarms* from those that are possibly associated to *fractures*, which require the visual inspection by the geophysicists. Bursts separation is performed by a classifier trained on bursts manually annotated by an experienced geophysicist. The burst-classification workflow is depicted in Figure VIII-C.

The intelligent mechanism at the Control Room, whose algorithm is shown in Alg. 1, operates as follows: as soon as a new burst arrives at the Control Room, it is automatically aligned and then processed to extract relevant features. Then, Linear Discriminant Analysis (LDA) [30] is applied to the extracted features to quantitatively assess to which extent the burst indicates a false alarm (that can be safely ignored) or a possible fracture (requiring the geophysicist intervention).

1) Burst Alignment: Let X_i be the 128 $\times$ 3 matrix corresponding to the raw measurements of the i-th burst as acquired by the three channel MEMS of the SPUs (we assume L=128 measurement per axis as shown in Table III). Of course, X_i depends on the SPU orientation and location since, in different SPUs, the MEMS axes are set along different orientations. During the alignment, X_i is transformed into a position-independent burst S_i to be compared with bursts acquired from different SPUs. Such alignment is performed via the Principal Component Analysis (PCA) [32] as follows:

$$S_i = X_i^0 W_i \tag{2}$$

where X_i^0 is the zero-centered matrix, and W_i is the 3 $\times$ 3 matrix corresponding to the eigenvectors of $(X_i^0)^T X_i^0$, where $()^T$ denotes the matrix transpose. The matrix X_i is thus projected into an orthonormal system identified by its principal components, and the aligned burst S_i corresponds to the scores of X_i.

It is worth mentioning that burst alignment by means of a preliminary calibration is not a viable option: mapping each burst into a common reference axis does not allow a meaningful analysis since the burst orientation depends on the SPU position w.r.t. the fracture source. In contrast, the proposed solution transforms each burst in an adaptively-defined orthonormal system, where the burst components are ordered depending on their magnitude (variance).

2) Feature Extraction: Features are compact descriptors of bursts, and provide essential information to determine whether X_i represents a false alarm or a possible fracture. In practice, feature extraction consists in computing a (real-valued) feature vector F_i extracted from each aligned burst S_i.

Nine independent features, summarized in Table IV, are extracted from each component of the aligned bursts, i.e., from each column of S_i (except made for the mean-before PCA which is the mean of X_i on each axis, projected into

Input: LDA projection vector a, matrix X_i of a bust to be analyzed (each component is a column)
1. Compute X_i^0 having zero-mean on each component
2. Define the matrix W_i, whose columns are the eigenvectors of $(X_i^0)^T X_i^0$, i.e, the principal components of X_i
3. Compute the aligned burst $S_i = X_i^0 W_i$
4. Compute the feature vector F_i, from the first and third columns of S_i
5. Compute the LDA projection $m_i = aF_i$
6. **if** $m_i < \Gamma_B$ **then**
7. $\quad$ X_i is considered a false alarm

else
8. $\quad$ X_i has to be analyzed by a geophysicist

end

Algorithm 1: Intelligent Mechanisms to separate bursts.

TABLE IV
FEATURES EXTRACTED FROM EACH (ALIGNED) BURST COMPONENT.

Time-domain features	Fourier-spectrum features
Mean (before PCA)	Spectrum amplitude
PCA eigenvalue	Main frequency
Signal Amplitude	Variance of spectrum peaks
Signal-to-noise ratio (SNR)	
Peak SNR (PSNR)	
Peak decay	

the principal component space). Features span both the time and Fourier domain. The noise standard deviation, which is used to compute the signal-to-noise ratio (SNR) and the peak signal-to-noise ratio (PSNR), is computed as in [33] using the median of absolute deviation estimator. The peak decay corresponds to the slope of the line joining the highest peak and the second highest peak. In Fourier domain, the variance of spectrum peaks is introduced as an indirect measure of how far the spectrum is from being unimodal.

We achieved satisfactory discriminative capability by considering only features from the principal and the less significant components of S_i. It follows that each burst X_i is described by a 18-dimensional feature vector F_i.

3) Burst Separation: This last phase associates to each burst a measure expressing to which extent it indicates a false alarm or a possible fracture. Such a measure is entirely computed in the feature domain via Linear Discriminant Analysis configured during the initial training phase.

LDA is a very popular classification algorithm that performs dimensionality reduction by linearly projecting input samples into the subspace where classes are better separated by an hyperplane. For binary classification problems, the target subspace is one-dimensional, and the projection corresponds to the inner product against a vector a, computed from the training set. Thus, LDA projects each 18-dimensional feature vector F_i into a scalar measure m_i, which indicates how close F_i is to the false alarms or to potentially relevant bursts:

$$m_i = aF_i. \tag{3}$$

Then, m_i is used as an indicator of the degree to which the burst is a false alarm: bursts yielding m_i values below the threshold Γ_B can be safely considered false alarms and discarded (as illustrated in Section IX-C). Large values of Γ_B could result in discarding true bursts, while low values would result in the processing of a very high number of false positive detections.

We chose LDA because its simple model reduces the risk of overfitting the training set; this aspect has to be taken into account as the feature dimension is rather large, and the number of bursts cannot be arbitrarily increased. Of course, the LDA projection vector a can be recomputed whenever additional supervised burst are available to improve the effectiveness of burst separation as in Eq. (3).

IX. Evaluation of the System Performance

The section aims at evaluating the performance of the proposed system in terms of the schedulability of the tasks in execution, clock synchronization and intelligent processing.

A. Tasks running at the SPUs: the schedulability analysis

The *schedulability analysis* verifies whether the execution of all tasks running at the SPUs (described in Section VIII-A) grants the real-time constraint to be satisfied (or not) [34]. At first, we recall that the considered real-time FreeRTOS OS is preemptive and based on the Rate Monotonic fixed-priority scheduling algorithm. Each task is characterized by a priority and by execution and deadline times. The priority value is fixed and set at *design-time*. Tasks with a lower value of priority can be preempted by tasks characterized by larger priority values. The execution time, namely the time necessary to execute the task, has been computed by considering the assembly-language version of the code and the execution time of the involved instructions. The deadline time defines the time instant by which the execution of all tasks must be completed.

Task ID	Responsibility	Priority	Duration (μs)	Deadline (μs)	R (μs)	Stack size (*bytes*)
T1	Filtering/event extraction (periodic)	1	267	500	267	420
T2	Parameter update (sporadic)	2	9.6	500	276.6	420
T3	Local synchronization (periodic)	3	110	500	386.6	630
T4	CAN driver (sporadic)	4	81.6	500	468.2	630
T5	Low level protocol FSM (sporadic)	5	51.4	100000	987.8	1050
T6	Watchdog (periodic)	7	7.8	500000	6499.8	420

TABLE V
DESCRIPTION, PRIORITY, DURATION, DEADLINE, R VALUE AND STACK SIZE OF THE TASKS RUNNING AT THE SPUS

The list of the tasks composing the SPU application (ordered by decreasing priority) is given in Table V. Some tasks are periodically executed by the SPU application (e.g., acquisition and processing, local communication, watchdog), while other tasks (e.g., parameter update, routing protocol) are triggered by external events such as communication interrupts or timeouts.

In particular, Task T1 represents the acquisition and processing task of the SPU described in Section VIII-A. This task is periodically executed every time a new set of samples is ready to be processed. As such, the deadline time of T1 is determined by the inter-sampling interval, i.e., 500μs, which sets a strong constraint and, therefore, the task is assigned the highest priority.

Task T2 is triggered by the push-parameters routing protocol of the reconfiguration service described in Section VII-A. This task updates the parameters of the SPU and its execution can be postponed after the completion of task T1 but must be completed before a new set of samples is acquired. As a consequence, the deadline time for T2 is set to 500μs.

Task T3 is executed only if the SPU is a Local Synchronization master. Similarly to T2, this periodic task, which sends the synchronization message to all other SPUs on the CAN bus every three seconds, must terminate before the new set of samples is acquired. Even in this case the deadline is 500μs.

The communication task is organized into two sub-tasks: T4 and T5. T4 is the CAN driver task, while T5 represents the routing protocol for the CAN bus as explained in Section VI-A. All these tasks are activated with low frequency. The deadline of T4 is 500μs to guarantee that each message is sent within the inter-sampling interval, while the deadline for task T5 is 1s. Finally, task T6 is a periodic task that resets the watchdog of the micro-controller. T6 must end before the watchdog fires and its deadline is fixed to 0.5s.

To evaluate the schedulability of the tasks running on the SPU we rely on the theoretical framework outlined in [34]. For the i-th task we compute the worst-case execution time

Memory Type	Available (kB)	Occupation (kB)
RAM	30720	30252 (5710 stack segment and 24542 data segment)
ROM	262144	48477 (code segment)

TABLE VI
MEMORY OCCUPATION OF THE SPUS

$R_i = C_i + B_i + I_i$, where C_i is the worst case computation time required by the task, B_i is the worst case blocking time as defined in [35] and I_i is the worst case interference that such task would experience from higher priority tasks. The computation of I_i and R_i is described in [34].

The schedulability of the tasks is guaranteed if all the worst-case execution times R_is are below their respective deadline times. As shown in Table V all the tasks satisfy this constraint, hence guaranteeing the schedulability of the SPU application tasks.

In addition, we evaluated the memory consumption of the SPU application. This analysis is of critical importance since the micro-controller at the SPU is characterized by limited ROM and RAM memory (as described in Section IV). This led us to consider a manual allocation of data-structures in memory (by modifying the compiler linker script) to exploit the available RAM memory as much as possible. Table VI summarizes the available and occupied RAM memory (i.e., total occupation, stack and data segment) and ROM memory (i.e., code segment). We emphasize that the manual allocation of the data-structures in memory allowed us to exploit up to 98% of the available RAM memory. Moreover, the last column of Table V shows the sizes of the memory stack assigned to each task. It is worth noting that T5 requires the largest amount of stack memory since it implements the PUSH/PULL protocols described in Section VI-A.

B. Synchronization mechanism

Here, we evaluate the effectiveness of the synchronization mechanism described in Section VII-C. Having this in mind we designed an experimental setup composed of a BS, three SPUs and a signal function generator. The BS is connected to the three SPUs through the CAN bus. The three SPUs run the same SPU application with the same parameters. *SPU1* is configured as the local synchronization master, while *SPU2* and *SPU3* are configured as slave units. The Agilent 33220A function generator was used to generate a voltage pulse every 15s with an amplitude of 3.3V and a time duration of 100ms. The function generator is connected to both *SPU2* and *SPU3* through the ADC channel corresponding to a channel of the MEMS accelerometer. With this experimental setup, both SPUs detect synthetically-generated events *at the same time*. We evaluated the effectiveness of the proposed synchronization service by measuring the clock skew between *SPU2* and *SPU3* over time by regularly polling both SPUs and comparing the timestamps associated with the detected events. All the experiments have been performed in our lab at a constant temperature.

At first, we considered the case where no synchronization service is employed and *SPU2* and *SPU3* have been synchronized only at the beginning of the experiment. These experimental results are presented in Fig. 7. We can observe a clock skew between the considered SPUs: the internal clock of *SPU3* runs slower than that of SPU2, hence increasing the clock skew over time. We recall that, as pointed out in Section VIII, the rock collapse forecasting application requires the clock skew among SPUs not to exceed 1ms. Experimental results are interesting since, as depicted in Fig. 7(b) detailing the time horizon of the first 400s, they show that without any synchronization mechanism between the SPUs the constraint on the clock skew (here emphasized by the black line) is no more satisfied after about 60 seconds.

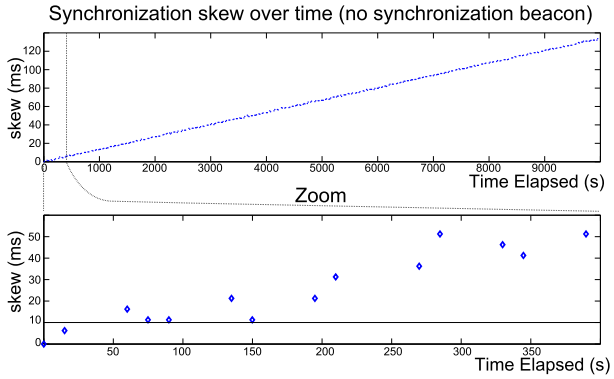

Fig. 7. Clock skew between *SPU2* and *SPU3* over time. Top: the time horizon of the analysis is 10000s. Bottom: the analysis focuses on the first 400s.

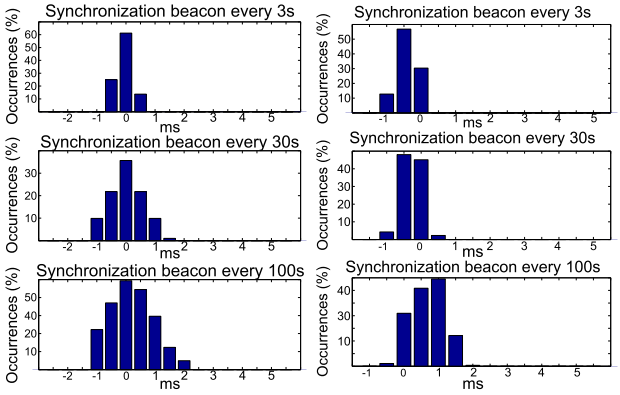

(a) 125kbs (b) 250kbs

Fig. 8. Histograms for the synchronization skew for different CAN bus baud rates

Then, we considered a synchronization mechanism with synchronization periods, i.e, the time between the activation of two subsequent synchronization services, ranging from 3s to 100s and different baud-rates for the CAN bus. Fig. 8 shows the experimental results wih baud-rate fixed at 125kbps and 250kbps. These figures show the histograms of the measured clock skew between *SPU2* and *SPU3* as a result of 300 experiments. Several comments arise. At first, in all the considered configurations of the baud-rate, the synchronization period of 3s guarantees the constraint on the clock skew to be largely satisfied. Second, as expected, the maximum value of the clock skew increases with the synchronization period. These results are in line with those of Fig. 7 and show that the 1ms constraint

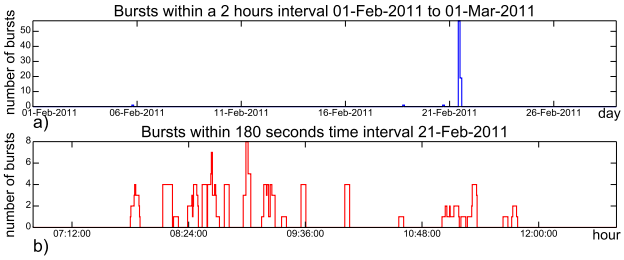

Fig. 9. Bursts recorded by the system deployed at Towers of Rialba in February 2011. Top: the number of bursts received by the BS every 2 hours (the time between two consecutive connections in normal transmission mode). Bottom: the number or bursts received in windows of $W_B = 180s$

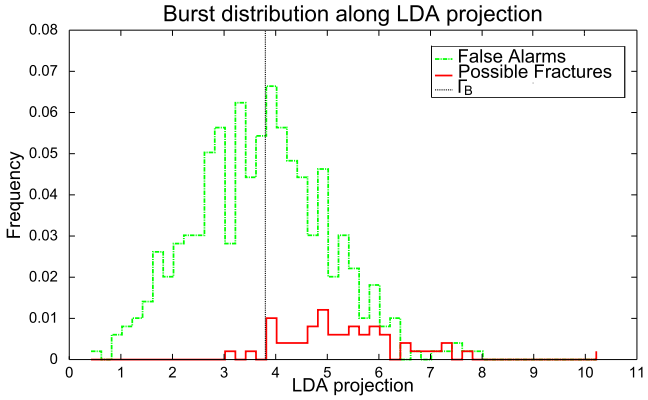

Fig. 11. Distribution of LDA values for bursts corresponding to possible fractures and false alarms.

is not satisfied with synchronization periods equal or larger than 60s. For example, given a synchronization period of 100s, the clock skew between *SPU2* and *SPU3* can be up to 2ms. Third, experimental results show that the baud-rate has no (or very little) influence on the measured clock-skew. This is in line with what presented in Section VII-C. In fact, the delay T_d induced by the transmission on the CAN bus is compensated via software according to the CAN bus baud-rate. In our real-world deployments, we opted for a conservative choice of the synchronization period fixing it to 3s (the baud-rate of the CAN bus is 250kbps).

C. Intelligent processing

We report some analysis on the bursts recorded by the deployment at Towers of Rialba [1]. Fig. 9a) illustrates the bursts arrivals in February 2011: each bin reports the number of bursts recorded in two hours, which is the temporal distance between two remote communications when the BS is in normal transmission-mode. The highest peak is caused by an artificially induced fracture in the rock face on Feb. 21: Fig. 9b) details the bursts acquired in this day reporting the number of bursts on windows lasting $W_B = 180$s. The set up of the equipment resulted in the generation of two sets of burst. The first set must be intended as false alarms introduced by the operators, while the last set is associated with the actual fracture: in both situations the BS entered in the alarm transmission-mode.

To illustrate the performance of the burst-separation algorithm presented in Section VIII-C we consider a dataset of 497 bursts recorded over more than two years of monitoring activity. Geophysicists visually inspected the whole dataset, classifying each of them either as bursts indicating false alarms (445 bursts) or possible fractures (52 bursts).

Fig. 10 plots the values of the LDA projection computed on all the bursts of the dataset. To ease the visualization, the dataset has been organized to report all the possible fractures at the beginning (followed by false alarms), and group bursts recorded from the same node (i.e., different markers are used for node 1, node 2 and node 3). Therefore, the burst index on the horizontal axis does not reflect the burst time-arrival. The vertical axis reports the values of the LDA projection of the respective burst. This figure clearly shows that the separation between possible fractures (corresponding to the initial 52 markers) and false alarms (corresponding to the rest of the markers) in the LDA projections is rather clear. Fig. 10 shows also two bursts (one associated with a fracture and one with a false alarm) and their LDA projection values to illustrate the difference between false alarms and possible fractures.

Burst separability is shown in Fig. 11, which presents the empirical distribution of the LDA projection values, computed on the whole dataset. This figure suggests that a suitable false positive filtering-strategy is effective and reduces the bursts to be visually inspected by the geophysicist to those yielding LDA projection above $\Gamma_B = 3.8$. Bursts yielding values of the LDA projections smaller than Γ_B can be safely ignored, as these in the 98% of cases correspond to a false alarm. Such a selection scheme allows to significantly reduce the number of bursts requesting the geophysicist intervention. The analysis will hence be focused on the remaining 50% of the bursts taking into account that approximately 19% of these correspond to possible fractures. These percentages can be modified by tuning threshold Γ_B.

X. Conclusions

The aim of this paper is to describe a reprogrammable and intelligent rock collapse forecasting system. The proposed forecasting system guarantees high-performance processing of high-frequency data directly at the unit level together with an effective and efficient analysis of acquired signals to identify and extract micro-acoustic emissions (that represent possible forerunners of a rock collapse). In addition the proposed system guarantees both a strict synchronization among the acquisition units (which is crucial for subsequent analyses of data at the control room) and the ability to remotely reconfigure of the applications running at the units and at the base station. The system has been successfully deployed in several areas of the Swiss-Italian Alps to forecast rock falls.

Acknowledgment

The authors would like to thank Dr. Ing. Romolo Camplani and Dr. Ing. Antonio Marullo for the precious contribution in the design and development of the proposed system.

[1]The dataset of acquired bursts is made available to the scientific community at the following web page: http://roveri.faculty.polimi.it/wp-content/uploads/bursts.zip

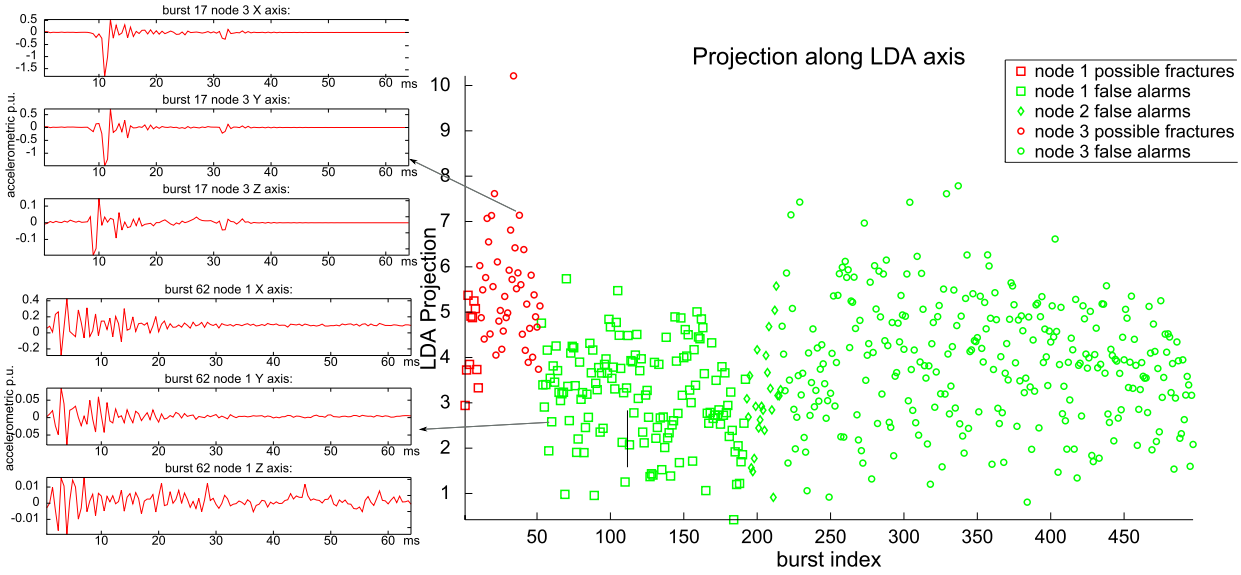

Fig. 10. Burst features projected along the LDA axis. The first 52 markers indicate bursts corresponding to possible fractures, while the remaining markers indicate false alarms. Different markers indicate the node that recorded the burst. The LDA values of bursts corresponding to possible fractures are typically larger than those corresponding to false alarms, indicating that these two classes can be separated.

REFERENCES

[1] O. Bukhalo, "Measuring transformations of acoustic emission signals," *Measurement Techniques*, vol. 45, pp. 966–973, 2002.

[2] C. Alippi, R. Camplani, C. Galperti, A. Marullo, and M. Roveri, "A high frequency sampling monitoring system for environmental and structural applications," *ACM Transactions on Sensor Networks*, 2013.

[3] ——, "An hybrid wireless-wired monitoring system for real-time rock collapse forecasting," in *Int. Conf. MASS*, nov. 2010, pp. 224 –231.

[4] L. Girard, J. Beutel, S. Gruber, J. Hunziker, R. Lim, and S. Weber, "A custom acoustic emission monitoring system for harsh environments: application to freezing-induced damage in alpine rock walls," *Geoscientific Instrumentation, Methods and Data Systems*, vol. 1, no. 2, pp. 155–167, 2012.

[5] A. Basharat, N. Catbas, and M. Shah, in *Workshops PerCom 2005*.

[6] P. Levis, S. Madden, J. Polastre, R. Szewczyk, K. Whitehouse, A. Woo, D. Gay, J. Hill, M. Welsh, E. Brewer *et al.*, "Tinyos: An operating system for sensor networks," *Ambient intelligence*, vol. 35, 2005.

[7] S. Ganeriwal, R. Kumar, and M. Srivastava, "Timing-sync protocol for sensor networks," in *Proc. Int. Conf. on Embedded Networked Sensor Systems*. ACM, 2003, pp. 138–149.

[8] e. a. Xu, Ning, "A wireless sensor network for structural monitoring," in *Proc. Int. Conf. on Embedded networked sensor systems*. ACM, 2004, pp. 13–24.

[9] S. Kim, S. Pakzad, D. Culler, J. Demmel, G. Fenves, S. Glaser, and M. Turon, "Health monitoring of civil infrastructures using wireless sensor networks," in *Int. Conf. on Information processing in sensor networks*. ACM, 2007, pp. 254–263.

[10] M. Maróti, B. Kusy, G. Simon, and Á. Lédeczi, "The flooding time synchronization protocol," in *Proc. Int. Conf. on Embedded Networked Sensor Systems*. ACM, 2004, pp. 39–49.

[11] E. Sazonov, K. Janoyan, and R. Jha, "Wireless intelligent sensor network for autonomous structural health monitoring," in *Smart Structures and Materials*. Int. Soc. for Optics and Photonics, 2004, pp. 305–314.

[12] M. Bocca, L. M. Eriksson, A. Mahmood, R. Jäntti, and J. Kullaa, "A synchronized wireless sensor network for experimental modal analysis in structural health monitoring," *Computer-Aided Civil and Infrastructure Engineering*, vol. 26, no. 7, pp. 483–499, 2011.

[13] S. Glaser, "Terra-Scope: a MEMS-based vertical seismic array," *Proc. SPIE*, 2005.

[14] G. Werner-Allen, K. Lorincz, M. Welsh, O. Marcillo, J. Johnson, M. Ruiz, and J. Lees, "Deploying a wireless sensor network on an active volcano," *IEEE Internet Computing*, pp. 18–25, 2006.

[15] M. Farooq and T. Kunz, "Operating systems for wireless sensor networks: A survey," *Sensors*, vol. 11, no. 6, pp. 5900–5930, 2011.

[16] e. a. Han, C.C., "SOS: A dynamic operating system for sensor networks," in *Int. Conf. on Mobile Systems, Applications, And Services*, 2005.

[17] FreeRTOS, "http://www.freertos.org/," in *The FreeRTOS Project*, 2011.

[18] W. Lawrenz, *Can System Engineering: From Theory to Practical Applications*, 1st ed. Springer-Verlag New York, Inc., 1997.

[19] "CIA," http://http://www.can-cia.org.

[20] "DeviceNet," http://ab.rockwellautomation.com/.

[21] "CAN Kingdom," http://www.kvaser.com/.

[22] K. Aberer, M. Hauswirth, and A. Salehi, "A middleware for fast and flexible sensor network deployment," in *Proc. Int. Conf. on Very large data bases*. VLDB Endowment, 2006, pp. 1199–1202.

[23] T. Luckenbach, P. Gober, S. Arbanowski, A. Kotsopoulos, and K. Kim, "Tinyrest-a protocol for integrating sensor networks into the internet," in *Proc. of REALWSN*, 2005.

[24] J. Sousa and D. Garlan, "Aura: an architectural framework for user mobility in ubiquitous computing environments," 2002.

[25] M. Román, C. Hess, R. Cerqueira, A. Ranganathan, R. Campbell, and K. Nahrstedt, "Gaia: a middleware platform for active spaces," *ACM SIGMOBILE Mobile Computing and Communications Review*, vol. 6, no. 4, pp. 65–67, 2002.

[26] F. Schreiber, R. Camplani, M. Fortunato, M. Marelli, and G. Rota, "Perla: A language and middleware architecture for data management and integration in pervasive information systems," *Software Engineering, IEEE Transactions on*, vol. 38, no. 2, pp. 478 –496, march-april 2012.

[27] D. L. Mills, "Internet time synchronization: the network time protocol," *Communications, IEEE Trans. on*, vol. 39, no. 10, pp. 1482–1493, 1991.

[28] " International Telecommunications Union," ITU Radiocommunication Assembly 2002.

[29] C. Alippi, *Intelligence for Embedded Systems*. Springer, 2014.

[30] T. Hastie, R. Tibshirani, and J. H. Friedman, *The elements of statistical learning: data mining, inference, and prediction: with 200 full-color illustrations*. Springer-Verlag, New York, February 2009.

[31] C. Alippi, R. Camplani, and C. Galperti, "Lossless compression techniques in wireless sensor networks: Monitoring microacoustic emissions," in *ROSE*. IEEE, 2007, pp. 1–5.

[32] R. Johnson and D. Wichern, *Applied multivariate statistical analysis*, 6th ed. Prentice Hall, April 2007, no. v. 1.

[33] D. L. Donoho and J. M. Jonstone, "Ideal spatial adaptation by wavelet shrinkage," *Biometrika*, vol. 81, no. 3, pp. 425–455, 1994. [Online]. Available: http://biomet.oxfordjournals.org/content/81/3/425.abstract

[34] N. Audsley, A. Burns, M. Richardson, K. Tindell, and A. Wellings, "Applying new scheduling theory to static priority pre-emptive scheduling," *Software Engineering Journal*, vol. 8, no. 5, pp. 284 –292, sep 1993.

[35] L. Sha, R. Rajkumar, and J. Lehoczky, "Priority inheritance protocols: An approach to real-time synchronization," *Computers, IEEE Transactions on*, vol. 39, no. 9, pp. 1175–1185, 1990.